Dynamic Current Control to Compensate for Magnetic Mutual Coupling in Electrically Excited Synchronous Machines

Dynamic Current Control to Compensate for Magnetic Mutual Coupling in Electrically Excited Synchronous Machines

Junfei Tang, *Student Member, IEEE*, and Yujing Liu, *Senior Member, IEEE*

***Abstract* – Electrically excited synchronous machines have become an attractive solution to electric vehicles. Equipped with a field winding in the rotor, the excitation of the machine is controllable. However, due to the magnetic mutual coupling between the stator and rotor windings, a voltage will be induced in the field winding in case of a current rise in the stator winding and vice versa. In this study, a dynamic current control algorithm with compensation for magnetic mutual coupling is proposed. A first-order response of current rise is expected. To achieve this, the controller consists of three parts. The first part is the feed forward of cross-coupling terms due to Park transform. The second part takes care of the resistances and self-inductances. The third part takes care of the mutual inductances. Finally, the outputs from the three parts are summed up to be the total output from the controller.**

***Index Terms*— Electrically excited synchronous machine, dynamic current control, magnetic mutual coupling.**

I. Introduction

Electric vehicles (EVs) have become a fast-growing area due to concerns of climate change [1]. Electric machines are key components in EV propulsion systems where permanent magnet synchronous machines (PMSMs) are a prevalent solution. In PMSMs, the main flux is generated from rare-earth magnets placed in the rotor. Due to the high level of maximum energy product of rare-earth magnets, high torque density can be achieved by utilizing PMSMs in EVs [2].

Nevertheless, rare-earth magnets are expensive. The extraction and refinement process of rare-earth magnets are not environmentally friendly [3]. Moreover, the recycling of rare-earth materials is complicated and still immature [4]. Comparably, in electrically excited synchronous machines (EESMs), a field winding is employed in the rotor. This means the machine is free of rare-earth materials. Additionally, the excitation of the machine is controllable by adjusting the field current [5]. As the consequence, high starting torque and wide field weakening range can be achieved by utilizing EESMs in EV applications [6].

Studies focusing on current control of EESMs have been pursued. In study [7], the target is to minimize the total amount of copper losses. Analytical solutions and iteration algorithms have been developed in case of normal operation, field-weakening and torque-boosting. In study [8], to minimize copper losses in field-weakening, a hybrid approach with analytical calculation, iterative computation and curve fitting is proposed. In study [9], loss minimization, torque response, thermal performance and safety requirements are investigated. In study [10], the torque-speed envelop and the corresponding trajectory of current vector in dq-frame are derived and presented. The performance of the drive is experimentally evaluated. The efficiency is higher than that of an induction machine drive while slightly lower than that of a PMSM drive. In study [11], deadbeat-direct torque and flux control for EESMs is proposed. Current and flux linkage observers are derived in discrete-time domain. The torque transient response is distributed between stator and rotor depending on voltage constraints. A predictive control algorithm is developed in study [12]. The torque can be inversed by inverting the excitation current. In study [13], an EESM is used as a generator in electric aircraft power system. A predictive control algorithm is developed in which parameter variations are taken into consideration.

The previous studies regarding current control are extensive. However, there is still one challenge not covered yet. Due to the magnetic mutual coupling between stator and field windings of an EESM, the current rise in one winding would induce an electromotive force (EMF) in the other. This will cause disturbances in current control, especially the control of d-axis current and field current. The traditional field-oriented control (FOC) of electric machines with loop-sharping design of proportional-integral (PI) regulators is a mature technology. Therefore, it is worth developing a dynamic current control algorithm based on FOC which takes the induced voltages due to mutual coupling into account.

Hence the aim of this study is to develop a dynamic current control algorithm to mitigate the disturbances due to mutual coupling for EESMs. In this article, the study is presented in three chapters. In the beginning, an electrical dynamic model of EESMs is established. Both self- and mutual inductances are included in the model. Then the dynamic current control algorithm is proposed. The controller consists of three parts in the algorithm. An anti-windup technique is introduced in case the voltage limits are reached. In the end, the dynamic current control is evaluated by connecting the controller with the electrical dynamic model of the machine. The EESM parameters used in the evaluation are from the finite element method (FEM) analysis results of an EESM design. Saturation of iron-cores are considered in this study by using look-up tables with interpolations in both machine modeling and controller design. Comparisons of performances are made between the cases with and without the compensation for mutual induced voltages. Thereafter, the necessity of the anti-windup technique in this control algorithm is demonstrated.

Junfei Tang is with Electric Power Engineering, Chalmers University of Technology, Gothenburg, Sweden (e-mail: junfei.tang@chalmers.se).

Yujing Liu is with Electric Power Engineering, Chalmers University of Technology, Gothenburg, Sweden (e-mail: yujing.liu@chalmers.se).

II. ELECTRICAL DYNAMIC MODEL OF MACHINE

The focus of this study is the dynamic current control for EESMs. Therefore, only the electrical dynamics of the machine are modeled while the mechanical speed of the machine is considered as constant. In this chapter, the electrical dynamics are modeled in dq-frame. The Park transform of electrical quantities from three-phase to dq-frame is amplitude-invariant. The field current is the actual dc current flows in the field winding without any scaling factor.

A. Electrical Dynamics

The electrical dynamics of the machine can be described in matrix form as

$$\boldsymbol{u} = \boldsymbol{R}\boldsymbol{i} + \boldsymbol{\omega}\boldsymbol{\psi} + \frac{d\boldsymbol{\psi}}{dt} \tag{1}$$

where $\boldsymbol{u}$, $\boldsymbol{i}$ and $\boldsymbol{\psi}$ are the vectors of voltages, currents and flux linkages in d-axis, q-axis and field

$$\boldsymbol{u} = \begin{bmatrix} u_\mathrm{d} \\ u_\mathrm{q} \\ u_\mathrm{f} \end{bmatrix}, \quad \boldsymbol{i} = \begin{bmatrix} i_\mathrm{d} \\ i_\mathrm{q} \\ i_\mathrm{f} \end{bmatrix}, \quad \boldsymbol{\psi} = \begin{bmatrix} \psi_\mathrm{d} \\ \psi_\mathrm{q} \\ \psi_\mathrm{f} \end{bmatrix} \tag{2}$$

$\boldsymbol{R}$ and $\boldsymbol{\omega}$ are the matrices of resistances and speed

$$\boldsymbol{R} = \begin{bmatrix} R_\mathrm{s} & 0 & 0 \\ 0 & R_\mathrm{s} & 0 \\ 0 & 0 & R_\mathrm{f} \end{bmatrix}, \quad \boldsymbol{\omega} = \begin{bmatrix} 0 & -\omega_\mathrm{r} & 0 \\ \omega_\mathrm{r} & 0 & 0 \\ 0 & 0 & 0 \end{bmatrix} \tag{3}$$

The term $\boldsymbol{\omega}\boldsymbol{\psi}$ here is named as cross-coupling EMF term, since in this term, d-axis flux linkage contributes to q-axis voltage and q-axis flux linkage contributes to d-axis voltage.

The derivatives of flux linkages can be further described as derivatives of currents

$$\frac{d\boldsymbol{\psi}}{dt} = \boldsymbol{L}\frac{d\boldsymbol{i}}{dt} \tag{4}$$

where $\boldsymbol{L}$ is a Jacobian matrix of incremental inductances

$$\boldsymbol{L} = \begin{bmatrix} L_\mathrm{dd} & L_\mathrm{dq} & L_\mathrm{df} \\ L_\mathrm{qd} & L_\mathrm{qq} & L_\mathrm{qf} \\ L_\mathrm{fd} & L_\mathrm{fq} & L_\mathrm{ff} \end{bmatrix} = \begin{bmatrix} \frac{\partial\psi_\mathrm{d}}{\partial i_\mathrm{d}} & \frac{\partial\psi_\mathrm{d}}{\partial i_\mathrm{q}} & \frac{\partial\psi_\mathrm{d}}{\partial i_\mathrm{f}} \\ \frac{\partial\psi_\mathrm{q}}{\partial i_\mathrm{d}} & \frac{\partial\psi_\mathrm{q}}{\partial i_\mathrm{q}} & \frac{\partial\psi_\mathrm{q}}{\partial i_\mathrm{f}} \\ \frac{\partial\psi_\mathrm{f}}{\partial i_\mathrm{d}} & \frac{\partial\psi_\mathrm{f}}{\partial i_\mathrm{q}} & \frac{\partial\psi_\mathrm{f}}{\partial i_\mathrm{f}} \end{bmatrix} \tag{5}$$

The flux linkages and inductances in this study are described by look-up tables so that iron-core saturation is taken into consideration. In steady state, the derivatives of currents in dq-frame are zero and therefore the derivatives of flux linkages in dq-frame are zero as well.

The incremental inductance matrix is composed by two parts, the self-inductance part

$$\boldsymbol{L}_\mathbf{self} = \begin{bmatrix} L_\mathrm{dd} & 0 & 0 \\ 0 & L_\mathrm{qq} & 0 \\ 0 & 0 & L_\mathrm{ff} \end{bmatrix} \tag{6}$$

and the mutual inductance part

$$\boldsymbol{L}_\mathbf{mutual} = \begin{bmatrix} 0 & L_\mathrm{dq} & L_\mathrm{df} \\ L_\mathrm{qd} & 0 & L_\mathrm{qf} \\ L_\mathrm{fd} & L_\mathrm{fq} & 0 \end{bmatrix} \tag{7}$$

The sum of them gives the total incremental inductance matrix

$$\boldsymbol{L} = \boldsymbol{L}_\mathbf{self} + \boldsymbol{L}_\mathbf{mutual} \tag{8}$$

The electromagnetic torque can be formulated as

$$T_\mathrm{em} = \frac{3}{2} \cdot p \cdot \left(\psi_\mathrm{d} \cdot i_\mathrm{q} - \psi_\mathrm{q} \cdot i_\mathrm{d}\right) \tag{9}$$

where p is the number of pole pairs.

B. Electrical Dynamic Model

The dynamic model is established based on the electrical dynamic process. The schematic diagrams of the model are illustrated in Fig. 1. The transforms between three-phase and dq-frame are considered as basics and not described here. The inputs, outputs, states and parameters are illustrated in Fig. 1 (a). To describe the electrical dynamics, the derivatives of flux linkages are firstly determined by reformulating (1) to

$$\frac{d\boldsymbol{\psi}}{dt} = \boldsymbol{u} - \boldsymbol{R}\boldsymbol{i} - \boldsymbol{\omega}\boldsymbol{\psi} \tag{10}$$

This process is illustrated in Fig. 1 (b). Then the derivatives of currents can be further determined through pre-multiplying $\frac{d\boldsymbol{\psi}}{dt}$ by the inverse of the inductance matrix

$$\frac{d\boldsymbol{i}}{dt} = \boldsymbol{L}^{-1}\frac{d\boldsymbol{\psi}}{dt} \tag{11}$$

Thereafter, the last step is to integrate the current derivatives and get the currents

$$\boldsymbol{i} = \int \frac{d\boldsymbol{i}}{dt} \cdot dt \tag{12}$$

This process is illustrated in Fig. 1 (c).

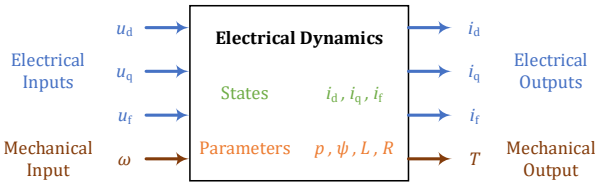

(a) Inputs, outputs, states and parameters of electrical dynamic model.

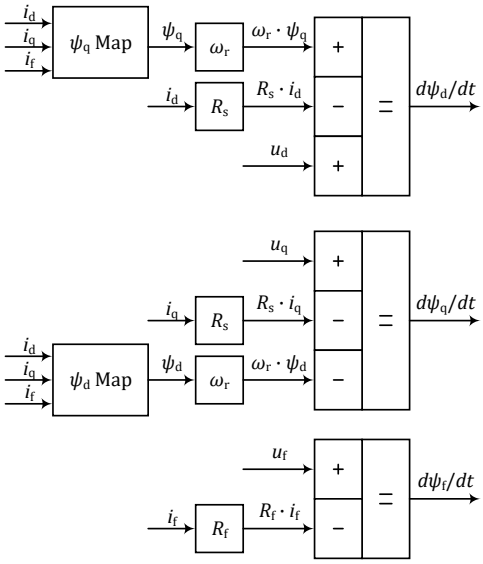

(b) Determination of flux linkage derivatives.

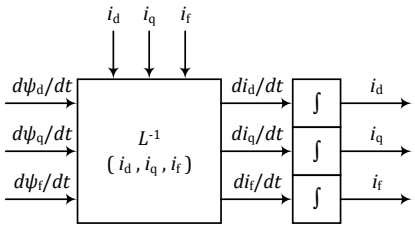

(c) Determination of currents.

Fig. 1 Schematic diagram of EESM dynamic model.

III. Dynamic Current Control

The aim of the dynamic current control is to form the step responses of current rises into the shape of first order. To achieve this, the controller is designed by taking care of three parts of the terminal voltage of the machine separately

$$\boldsymbol{u} = \boldsymbol{u}_{\text{self}} + \boldsymbol{u}_{\text{mutual}} + \boldsymbol{u}_{\text{cross}} \tag{13}$$

where $\boldsymbol{u}_{\text{self}}$ is the voltage across the resistances and self-inductances, i.e. in this part, the d-axis, q-axis and field circuits are independent, so it is actually a stacking of three single-input single-output (SISO) systems

$$\boldsymbol{u}_{\text{self}} = \boldsymbol{R}\boldsymbol{i} + \boldsymbol{L}_{\text{self}}\frac{d\boldsymbol{i}}{dt} \tag{14}$$

$\boldsymbol{u}_{\text{mutual}}$ is the voltage across the mutual-inductances, i.e. in this part, the d-axis voltage is decided by the q-axis and field current derivatives, the q-axis voltage is decided by the d-axis and field current derivatives and the field voltage is decided by the d-axis and q-axis current derivatives

$$\boldsymbol{u}_{\text{mutual}} = \boldsymbol{L}_{\text{mutual}}\frac{d\boldsymbol{i}}{dt} \tag{15}$$

$\boldsymbol{u}_{\text{cross}}$ is the cross-coupling part

$$\boldsymbol{u}_{\text{cross}} = \boldsymbol{\omega}\boldsymbol{\psi} \tag{16}$$

In terms of controller design, these three parts can be taken care of separately

$$\boldsymbol{u}_{\text{ctrl}} = \boldsymbol{u}_{\text{ctrl.self}} + \boldsymbol{u}_{\text{ctrl.mutual}} + \boldsymbol{u}_{\text{ctrl.cross}} \tag{17}$$

where $\boldsymbol{u}_{\text{ctrl}}$ is the total controller output, $\boldsymbol{u}_{\text{ctrl.self}}$, $\boldsymbol{u}_{\text{ctrl.mutual}}$ and $\boldsymbol{u}_{\text{ctrl.cross}}$ are the controller outputs for the self-, mutual and cross-coupling parts respectively.

A. Feedforward for Cross-Coupling Part

The cross-coupling part is an addition part

$$\boldsymbol{u}_{\text{ctrl.cross}} = \boldsymbol{u}_{\text{cross}} = \boldsymbol{\omega}\boldsymbol{\psi} \tag{18}$$

With this cross-coupling term fed forwarded, the remaining parts are RL circuits including resistances, self-inductances and mutual inductances.

B. Loop Shaping PI Regulator for Self-Part

The self-part is a stack of three RL circuits. For each RL circuit, a PI regulator can be designed to shape the current response into first order with a bandwidth of α_{c}. The risetime is defined as the time interval for the current to rise from 10% to 90% of the steady state level. The relation between the bandwidth α_{c} in rad/s and risetime t_{r} in s follows

$$t_{\text{r}} = \ln 9 \,/\alpha_{\text{c}} \tag{19}$$

To have a first-order response, the PI coefficients are set as

$$k_{\text{P}} = \alpha_{\text{c}} \cdot L \quad , \quad k_{\text{I}} = \alpha_{\text{c}} \cdot R \tag{20}$$

Hence the voltage applied across the self-part is

$$\boldsymbol{u}_{\text{ctrl.self}} = \boldsymbol{K}_{\text{P}}\boldsymbol{i}_{\text{err}} + \boldsymbol{K}_{\text{I}}\int \boldsymbol{i}_{\text{err}}dt \tag{21}$$

in terms of all the three RL circuits together, where

$$\boldsymbol{i}_{\text{err}} = \boldsymbol{i}_{\text{ref}} - \boldsymbol{i}_{\text{msr}} \tag{22}$$

$\boldsymbol{i}_{\text{ref}}$ are current references, $\boldsymbol{i}_{\text{msr}}$ are current measurements, $\boldsymbol{K}_{\text{P}}$ and $\boldsymbol{K}_{\text{I}}$ are matrices of PI coefficients

$$\boldsymbol{K}_{\text{P}} = \boldsymbol{A}_{\text{c}}\boldsymbol{L} \quad , \quad \boldsymbol{K}_{\text{I}} = \boldsymbol{A}_{\text{c}}\boldsymbol{R} \tag{23}$$

$\boldsymbol{A}_{\text{c}}$ is the matrix of control bandwidth

$$\boldsymbol{A}_{\text{c}} = \begin{bmatrix} \alpha_{\text{c.d}} & 0 & 0 \\ 0 & \alpha_{\text{c.q}} & 0 \\ 0 & 0 & \alpha_{\text{c.f}} \end{bmatrix} \tag{24}$$

and $\alpha_{\text{c.d}}$, $\alpha_{\text{c.q}}$ and $\alpha_{\text{c.f}}$ are the bandwidths of d-axis, q-axis and field current control respectively.

C. Compensation for Mutual-Part

The vector of current derivatives to form the desired first-order responses with bandwidths in (24) can be determined as

$$\frac{d\boldsymbol{i}}{dt} = \boldsymbol{L}_{\text{self}}^{-1}(\boldsymbol{u}_{\text{ctrl.self}} - \boldsymbol{R}\boldsymbol{i}_{\text{msr}}) \tag{25}$$

The self-inductance matrix is diagonal as shown in (6). Therefore, it is inversible, which means the solution of $\boldsymbol{L}_{\text{self}}^{-1}$ always exists. The current derivatives here are the ones decided by the controller to form first-order responses instead of the derivatives of current samplings which are noisy.

Then to achieve the target current derivatives in (25), the vector of voltages that needs to be applied across the mutual inductances can be determined as

$$\boldsymbol{u}_{\text{ctrl.mutual}} = \boldsymbol{L}_{\text{mutual}}\frac{d\boldsymbol{i}}{dt} \tag{26}$$

Combining (25) and (26), the vector of voltages applied across the mutual inductances is

$$\boldsymbol{u}_{\text{ctrl.mutual}} = \boldsymbol{L}_{\text{mutual}}\boldsymbol{L}_{\text{self}}^{-1}(\boldsymbol{u}_{\text{ctrl.self}} - \boldsymbol{R}\boldsymbol{i}_{\text{msr}}) \tag{27}$$

This shows the mutual induced voltages to be compensated for to form the target first-order current rises.

D. Another Perspective of the Control

The controller output voltage introduced in (17) can be described in another format

$$\boldsymbol{u}_{\text{ctrl}} = \boldsymbol{u}_{\text{ctrl.R}} + \boldsymbol{u}_{\text{ctrl.L}} + \boldsymbol{u}_{\text{ctrl.cross}} \tag{28}$$

where $\boldsymbol{u}_{\text{ctrl.R}}$ is the voltage vector applied across the resistances, $\boldsymbol{u}_{\text{ctrl.L}}$ is the voltage vector applied across the inductances and $\boldsymbol{u}_{\text{ctrl.cross}}$ is the feed forward of cross-coupling terms which is the same as described in (18). The voltage vector $\boldsymbol{u}_{\text{ctrl.R}}$ follows the Ohm's Law

$$\boldsymbol{u}_{\text{ctrl.R}} = \boldsymbol{R}\boldsymbol{i}_{\text{msr}} \tag{29}$$

The voltage vector $\boldsymbol{u}_{\text{ctrl.L}}$ is determined by the current derivatives to form first-order responses

$$\boldsymbol{u}_{\text{ctrl.L}} = \boldsymbol{L}\frac{d\boldsymbol{i}}{dt} = \boldsymbol{L}\boldsymbol{L}_{\text{self}}^{-1}(\boldsymbol{u}_{\text{ctrl.self}} - \boldsymbol{R}\boldsymbol{i}_{\text{msr}}) \tag{30}$$

The $\boldsymbol{u}_{\text{ctrl.self}}$ here is determined in the same way as in (21). From this perspective, the PI regulator described in (21) is a tool to determine the current derivatives targeting the shape of first-order responses. Then the current derivatives are further used to determine the voltage vector that needs to be applied across the total inductances.

E. Dynamic Control with Voltage Limit

The voltages applied across the windings are limited to the converter output capabilities. In case the voltage reference exceeds the limit, the voltage output is saturated. In this situation, the controller needs to be aware of this to avoid the integrator from winding up. This is the anti-windup technique.

In this study, since the PI regulator is only used to take care of the self-part of the winding, the anti-windup technique only needs to be applied accordingly there to avoid the windup of the integrator. The input to the integrator is then modified from $\boldsymbol{i}_{\text{err}}$ in (21) to

$$\boldsymbol{i}_{\text{err}} + \boldsymbol{K}_{\text{P}}^{-1}(\boldsymbol{u}_{\text{ctrl.self.lim}} - \boldsymbol{u}_{\text{ctrl.self}}) \tag{31}$$

Due to the limited voltage output capability during saturation, the feed forward of the d- and q-axis cross-coupling terms cannot function well even with the anti-windup technique implemented, so as the compensation for the induced voltages due to mutual coupling.

IV. Performance Evaluation

A. Machine and Converter

An EESM is designed with the assistance of finite element method (FEM) analysis. The machine is with 8 poles and 48 slots. The maximum levels of stator and field currents are decided by current densities of 15 A/mm^2 and 10 A/mm^2 respectively. The flux density distributions of the machine at no load and peak torque operations are shown in Fig. 2. The parameters of the machine are listed in TABLE I.

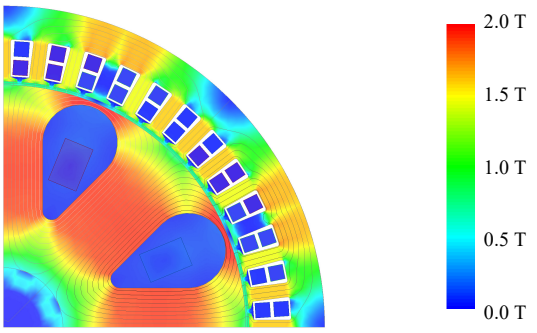

(a) No load operation.

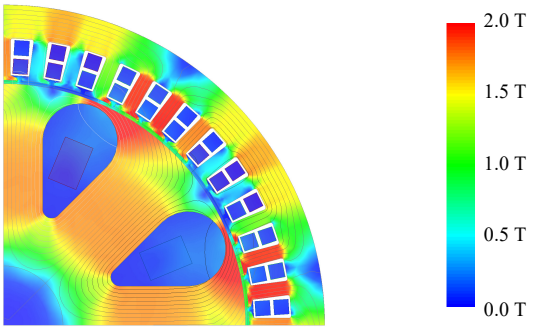

(b) Peak torque operation.

Fig. 2 Flux density distribution.

TABLE I
Machine Parameters

Parameter	Symbol	Value	Unit
lamination outer diameter	$d_{\text{s.outer}}$	270	mm
lamination stack length	L_{stack}	360	mm
peak torque	$T_{\text{em.max}}$	800	N·m
peak power	$P_{\text{em.max}}$	250	kW
maximum stator current amplitude @ current density of 15 A/mm^2	$I_{\text{s.amp.max}}$	450	A
maximum field current @ current density of 10 A/mm^2	$I_{\text{f.max}}$	7.854	A
stator resistance @ 100°C	R_{s}	19.55	mΩ
field resistance @ 100°C	R_{f}	54.71	Ω
d-axis self-inductance @ zero current	$L_{\text{dd·0}}$	1.30	mH
q-axis self-inductance @ zero current	$l_{\text{qq·0}}$	1.30	mH
field self-inductance @ zero current	$l_{\text{ff·0}}$	20.29	H
dq mutual-inductance @ zero current	$l_{\text{dq·0}}$	0.00	mH
df mutual -inductance @ zero current	$l_{\text{df·0}}$	92.80	mH
qf mutual -inductance @ zero current	$l_{\text{qf·0}}$	-3.58	μH

There are two power electronic converters in this study. One is a three-phase inverter which delivers power to the stator winding. Another one is a dc-dc H-bridge converter which delivers power to the field winding. These two converters share the same dc-link voltage source. Since the aspect of control is the focus of this study, the converters here are considered as ideal voltage sources without voltage drops across the switches or the transformer of the H-bridge converter. The parameters of the converters are listed in TABLE II. The voltage limit of the three-phase inverter is decided by considering only the linear modulation range.

TABLE II
Power Electronic Converters

Parameters	Symbol	Value	Unit
dc-link voltage	U_{dc}	800	V
transformer turns ratio of H-bridge converter	α_{T}	1:1	
three-phase voltage max	$U_{\text{s.amp.max}}$	462	V
field voltage max	$U_{\text{f.max}}$	800	V
field voltage min	$U_{\text{f.min}}$	0	V

B. Dynamic Current Control within Voltage Limit

The study is started with the simplest case in which the controller output voltages are within the converter output voltage limits. The bandwidths of the current control and the corresponding risetimes are listed in TABLE III. The current reference steps are defined in TABLE IV. The current steps are small compared with the current limits. This is to avoid the voltages from exceeding the limits. In this study, for the sake of convenience, the control taking care of only the self-inductances is noted as "Case 0" which means the original case, whereas the proposed control algorithm taking care of both the self- and mutual inductances is noted as "Case 1".

TABLE III
Parameters of Current Controller

Parameter	Bandwidth		Rise Time	
	Value	Unit	Value	Unit
d-axis current control	10	Hz	35	ms
q-axis current control	10	Hz	35	ms
field current control	5	Hz	70	ms

TABLE IV
Steps of Current References

References	From		To		At	
	Value	Unit	Value	Unit	Value	Unit
d-axis current step	0	A	50	A	0.7	s
q-axis current step	0	A	50	A	0.4	s
field current step	0	A	1	A	0.1	s

As a brief comparison of the results, the risetimes of the currents are measured and the bandwidths are calculated, as presented in TABLE V. The risetimes in Case 0 deviate from the target values as presented in TABLE III, whereas the risetimes in Case 1 closely follow the targets. This indicates that with mutual induced voltages compensated, first-order responses can be achieved. In addition, the rise times of the d-axis and field currents deviate more than that of the q-axis current. This is due to the higher mutual inductance between the d-axis and field than that between the q-axis and field.

TABLE V
CURRENT RESPONSE

Case	Quantity	Bandwidth		Rise Time	
		Value	Unit	Value	Unit
Case 0	d-axis current	7.15	Hz	48.88	ms
	q-axis current	9.96	Hz	35.12	ms
	field current	4.18	Hz	83.60	ms
Case 1	d-axis current	10.20	Hz	34.27	ms
	q-axis current	10.20	Hz	34.27	ms
	field current	5.10	Hz	68.55	ms

The step responses of the currents with (Case 1) and without (Case 0) compensations for mutual induced voltages are compared in Fig. 3 and Fig. 4. As already compared in TABLE V, the current responses in Case 1, i.e. the waveforms of $i_{\mathrm{d.msr.1}}$, $i_{\mathrm{q.msr.1}}$ and $i_{\mathrm{f.msr.1}}$ can be considered as first order. Discrepancies between the two cases are then pointed out and explained.

A disturbance in $i_{\mathrm{d.msr.0}}$ starting from 0.1 s can be noticed in Fig. 3 when the field current rises as shown in Fig. 4. The disturbance here is due to the EMF across L_{df} induced by the field current rise. This amount of induced voltage should be compensated for by the controller to keep the d-axis current at zero, but it is not in Case 0. Therefore, the d- and q-axis voltages deviate from how they should behave as shown in Fig. 5. The disturbance in d-axis current then affects the field current in return through an induced voltage across L_{fd}. The influence can be firstly seen in the deviation of field voltage shown in Fig. 6. Then it ends up with a discrepancy between $i_{\mathrm{f.msr.0}}$ and $i_{\mathrm{f.msr.1}}$ around 0.2 s shown in Fig. 4.

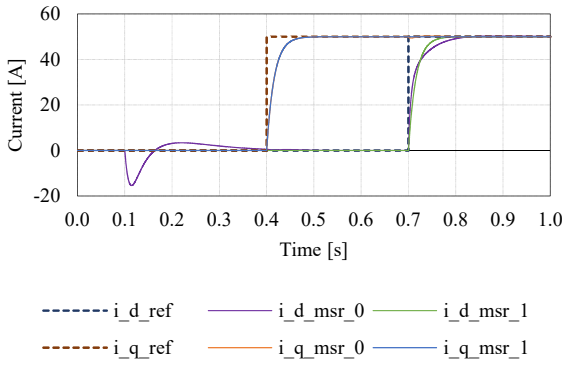

Fig. 3 Step responses of d- and q-axis current.

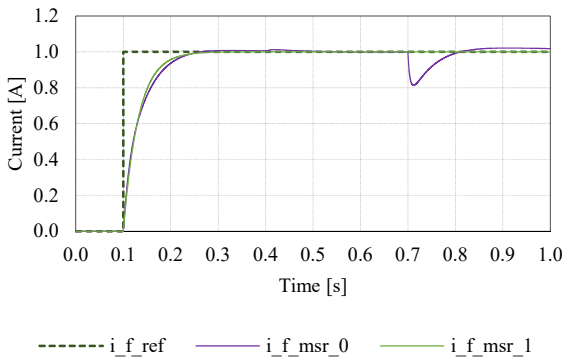

Fig. 4 Step response of field current.

At 0.7 s, the d-axis current rises, and a dip in $i_{\mathrm{f.msr.0}}$ can be noticed in Fig. 4. The explanation for this is similar to the one for the disturbance at 0.1 s in d-axis current. An EMF across L_{fd} is induced by the rise of d-axis current. The controller in Case 0 does not take this mutual induced voltage into account. Therefore, a dip appears in the field current. The field current controller detects the error and then gradually increases the voltage output as shown in Fig. 6 to turn the field current back as shown in Fig. 4. The disturbance in field current then induces an EMF in d-axis and affects the d-axis current in return as shown in Fig. 3.

The waveform of the electromagnetic torque is presented in Fig. 7. As can be noticed, the dip in field current shown in Fig. 4 causes a dip in torque as shown in Fig. 7. With mutual induced voltages compensated in Case 1, the torque response becomes smooth.

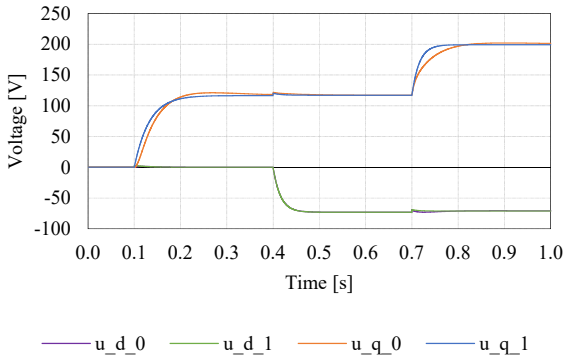

Fig. 5 Waveforms of d- and q-axis voltages.

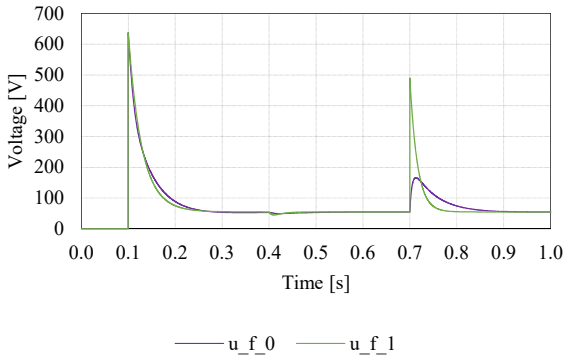

Fig. 6 Waveforms of field voltage.

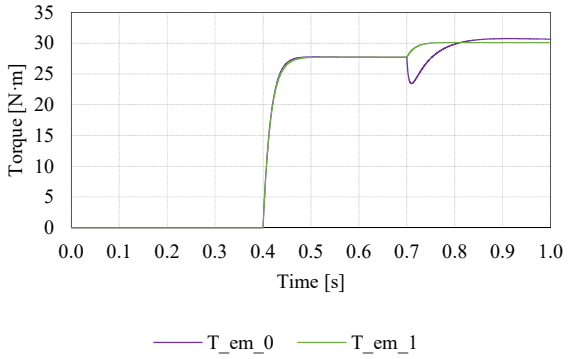

Fig. 7 Waveforms of electromagnetic torque.

C. *Dynamic Current Control with Voltage Limit Reached*

In this section, the control bandwidths are given as 10 times of the previous ones as listed in TABLE VI. The current references are given as the ones with which the machine delivers peak torque. The steps of current references are defined in TABLE VII. With these setups, the voltage limits would be hit when the currents step up. Two cases are studied in this section. One case is with no anti-windup implemented, named as "Case 2", whereas the other case is with anti-windup implemented, named as "Case 3".

TABLE VI
PARAMETERS OF CURRENT CONTROLLER

Parameter	Bandwidth		Rise Time	
	Value	Unit	Value	Unit
d-axis current control	100	Hz	3.5	ms
q-axis current control	100	Hz	3.5	ms
field current control	50	Hz	7.0	ms

TABLE VII
STEPS OF CURRENT REFERENCES

References	From		To		At	
	Value	Unit	Value	Unit	Value	Unit
d-axis current step	0	A	-131.8	A	0.05	s
q-axis current step	0	A	430.3	A	0.20	s
field current step	0	A	7.854	A	0.35	s

The stator and field current responses are presented in Fig. 8 and Fig. 9. The stator and field voltages can be seen in Fig. 10 and Fig. 11. In Fig. 8, the d-axis current in Case 2 is disturbed at 0.05 s. This happens when the field voltage hits the limit as can be seen in Fig. 11. In this situation, $\boldsymbol{u}_{\text{ctrl.self}}$ calculated in the controller exceeds the voltage limit. By using this exceeded voltage level of $\boldsymbol{u}_{\text{ctrl.self}}$, the current derivatives $\frac{di}{dt}$ are over-estimated, because the actual voltages applied across the self-inductances is limited but the controller is not aware of this. Consequently, unnecessarily higher voltages are applied across the stator windings as can be seen in Fig. 10. This causes the disturbance in d-axis current at 0.05 s.

After the d-axis current comes back to zero, it then goes to negative instead of staying at zero. This is due to the mechanism of PI control. A PI controller integrates the error to eliminate the error. A negative integral is established when the d-axis current goes to positive. To cancel this negative integral, the d-axis current needs to go negative for some time, and in the end, the negative area should be equal to the positive area enclosed by the current waveform and the time-axis.

The field current in Case 2 rises faster than that in Case 3 starting from 0.05 s. This is due to a negative EMF induced in the field winding by the decrease of the d-axis current. The induced negative EMF together with the applied field voltage at the terminal gives a higher voltage in total applied across the self-inductance in field winding. Consequently, the field current rises faster in Case 2.

A large over-shoot in field current can be observed in Case 2. This is due to two reasons. One reason is that, the PI regulator of the field current only takes care of the resistance and the self-inductance in the field winding. The EMFs across the mutual inductances are disturbances not considered in the PI regulator design. These EMFs cannot be canceled by the compensation algorithm either because the current derivatives

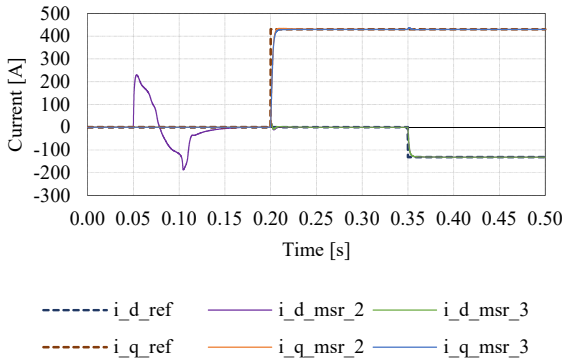

Fig. 8 Step responses of d- and q-axis currents.

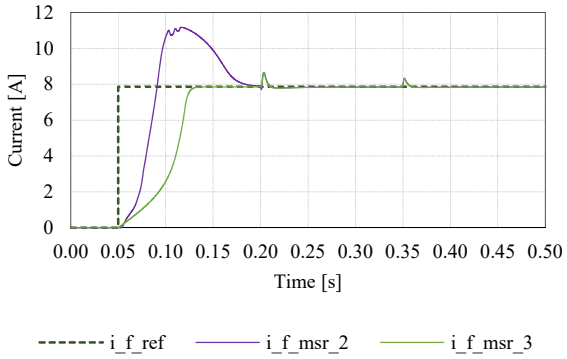

Fig. 9 Step response of field current.

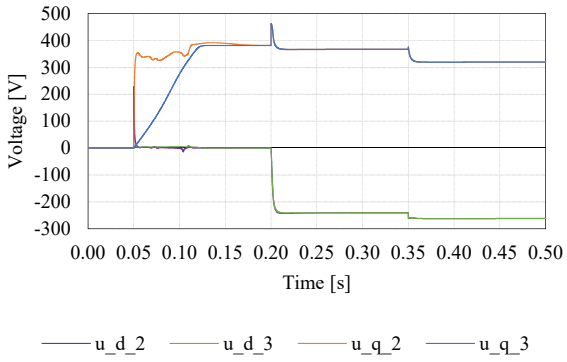

Fig. 10 Waveforms of d- and q-axis voltages.

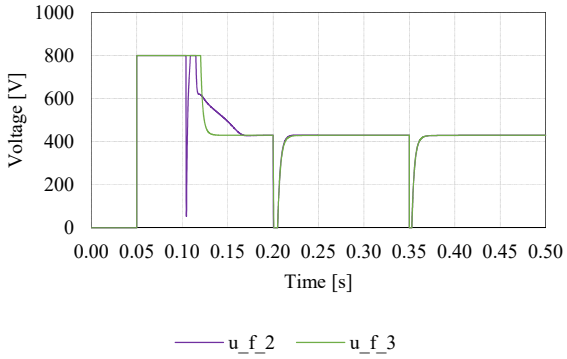

Fig. 11 Waveforms of field voltage.

are calculated based on $\boldsymbol{u}_{\mathrm{ctrl.self}}$ which is not the correct value when the voltage limit is hit. Another reason is that, anti-windup is not implemented in Case 2. Thus the integrator keeps integrating the entire amount of error current even after the voltage limit is hit. This means the integrator winds up. Hence after the field voltage exits saturation, it takes time for the integrator to clear this extra amount of integral.

In contrast to Case 2, the current waveforms in Case 3 are clean during the rise of field current. This is due to the anti-windup applied to $\boldsymbol{u}_{\mathrm{ctrl.self}}$. However, during the rises of d- and q-axis currents, the field current is disturbed even with anti-windup implemented as can be noticed in Fig. 9. This is due to that the EMFs in the field winding induced by d- and q-axis currents are too high for the field voltage to compensate for though the field voltage in terminal already drops to zero. As has been described in the design section, the compensation for the induced voltage due to mutual coupling cannot function well when the voltage output capability is already exhausted. Hence in this situation, the same disturbances appear in field current in both Case 2 and Case 3. In comparison, during the rise of field current, there is no disturbance in d- and q-axis currents. This is because the stator voltage output capability is not exhausted yet and the controller can still compensate for the induced voltages across the mutual inductances in the stator winding.

V. Conclusions

A dynamic current control algorithm for electrically excited synchronous machines has been proposed in this study. In the control algorithm, the induced voltages due to mutual coupling are compensated for during the transients of current rises. The rises of d-axis, q-axis and field currents are in the shape of first-order responses. Disturbances in current waveforms due to mutual coupling are mitigated and the current waveforms become clean. Consequently, the torque response becomes smooth compared to the case without compensations for mutual coupling. An anti-windup technique is implemented to avoid the integrator from winding up when the voltage limits are reached. It is shown in the analysis that the anti-windup technique is essential to make the compensations for mutual coupling work properly in case of voltage output saturation.

VI. References

[1] International Energy Agency, "Global EV Outlook 2019," International Energy Agency, 2019.

[2] J. D. Widmer, R. Martin and M. Kimiabeigi, "Electric Vehicle Traction Motors without Rare Earth Magnets," *Sustainable Materials and Technologies,* vol. 3, pp. 7-13, 2015.

[3] D. G. Dorrell, A. M. Knight, M. Popescu, L. Evans and D. A. Staton, "Comparison of Different Motor Design Drives for Hybrid Electric Vehicles," in *2010 IEEE Energy Conversion Congress and Exposition*, Atlanta, 2010.

[4] Y. Yang, A. Walton, R. Sheridan, K. Güth, R. Gauß, O. Gutfleisch, M. Buchert, B.-M. Steenari, T. V. Gerven, P. T. Jones and K. Binnemans, "REE Recovery from End-of-Life NdFeB Permanent MagnetScrap: A Critical Review," *Journal of Sustainable Metallurgy,* vol. 3, no. 1, pp. 3 - 30, 2017.

[5] J. Tang and Y. Liu, "Design and Experimental Verification of a 48 V 20 kW Electrically Excited Synchronous Machine for Mild Hybrid Vehicles," in *2018 XIII International Conference on Electrical Machines (ICEM)*, Alexandroupoli, 2018.

[6] J. Tang and Y. Liu, "Comparison of Copper Loss Minimization and Field Current Minimization for Electrically Excited Synchronous Motor in Mild Hybrid Drives," in *19th European Conference on Power Electronics and Applications (EPE'17 ECCE Europe)*, Warsaw, Poland, 2017.

[7] O. Haala, B. Wagner, M. Hofmann and M. März, "Optimal current control of externally excited synchronous machines in automotive traction drive applications," *International Journal of Electrical, Computer, Energetic, Electronic and Communication Engineering,* vol. 7, no. 9, pp. 1133 - 1139, 2013.

[8] Y. Kim and K. Nam, "Copper-Loss-Minimizing Field Current Control Scheme for Wound Synchronous Machines," *IEEE Transactions on Power Electronics,* vol. 32, no. 2, pp. 1335 - 1345, 2017.

[9] M. Märgner and W. Hackmann, "Control Challenges of An Externally Excited Synchronous Machine in An Automotive Traction Drive Application," in *2010 Emobility - Electrical Power Train*, Leipzig, 2010.

[10] C. Rossi, D. Casadei, A. Pilati and M. Marano, "Wound Rotor Salient Pole Synchronous Machine Drive for Electric Traction," in *Industry Applications Conference, 2006. 41st IAS Annual Meeting. Conference Record of the 2006 IEEE*, Tampa, 2006.

[11] Y. Nie, I. P. Brown and D. C. Ludois, "Deadbeat-Direct Torque and Flux Control for Wound Field Synchronous Machines," *IEEE Transactions on Industrial Electronics,* vol. 65, no. 3, pp. 2069 - 2079, 2018.

[12] P. Winzer, J. Richter and M. Doppelbauer, "Dynamic Control of Generalized Electrically Excited Synchronous Machines Using Predictive Flux Control," in *IECON 2016 - 42nd Annual Conference of the IEEE Industrial Electronics Society*, Florence, 2016.

[13] M. Alnajjar and D. Gerling, "Predictive Control of Variable Frequency Brushless Excited Synchronous Generator for More Electric Aircraft Power System," in *2014 International Conference on Electrical Machines (ICEM)*, Berlin, 2014.

VII. Biographies

Junfei Tang (S'16) received B.Eng. in electrical engineering from Jiangsu University, Zhenjiang, China, in 2013, and M.Sc. in electric power engineering from Chalmers University of Technology, Gothenburg, Sweden, in 2016. Now he is pursuing his doctoral study in electric machines and power electronics in Chalmers University of Technology.

Yujing Liu (SM'12) received B.Sc., M.Sc. and Ph.D. degrees in electrical engineering from Harbin Institute of Technology, Harbin, China, in 1982, 1985, and 1988, respectively. In 1996-2013, he worked in ABB Corporate Research, Västerås, Sweden. Since 2013, he is a professor on electrical power engineering in Chalmers University of Technology. Gothenburg, Sweden. His interest includes research on motors, converters, and wireless charging for electric vehicles, generators and power electronics for tidal power conversion, and high efficiency machines for energy saving in industrial applications. Yujing Liu is a senior IEEE member and a member in Swedish Standard Committee on Electrical Machines.